RESEARCH PAPER

Analysis of Zinc Oxide (ZnO) Thin nano Film Produced Using the Sol-Gel Method

*Lamis Faaz Nassir [1] *, Ahmed Shaker Hussein [2], Hiba Hussein Fadil Mahdi [3]*

[1] *Hammurabi College of Medicine, University of Babylon, Iraq*
[2] *College of Dentistry, University of Babylon, Iraq*
[3] *Faculty of Nursing, University of Babylon, Iraq*

ARTICLE INFO

Article History:
Received 03 January 2025
Accepted 25 March 2025
Published 01 April 2025

Keywords:
Optical properties
Sol-Gel method
X-Ray Diffraction
ZnO thin nano-films

ABSTRACT

In this study, the optical characteristics of zinc oxide (ZnO) thin nano films, deposited by the spray pyrolysis method have been investigated. A quartz substrate was heated to 350 °C in order to deposit a thin coating of ZnO. The film's structural properties were examined by X-ray diffraction (XRD) analysis, and its optical properties were determined by transmittance spectra; these properties can be fine-tuned by UV-Vis. spectroscopy to suit the film's intended uses in solar energy conversion and photovoltaic solar cell devices. Based on the results obtained by XRD, the deposited film is wurtzite, which has a hexagonal structure and a preferred orientation along the (002) crystal plane, as well as a broadened peak. Very high absorption values (90%) were observed in the ZnO nano-films. Further research on the ZnO nano-films revealed an optical band gap of 2.84 eV. These findings underscore the potential of spray pyrolysis-deposited ZnO nano-films for optoelectronic applications.

How to cite this article
Nassir L., Hussein A., Mahdi H. Analysis of Zinc Oxide (ZnO) Thin nano Film Produced Using the Sol-Gel Method. J Nanostruct, 2025; 15(2):555-562. DOI: 10.22052/JNS.2025.02.016

INTRODUCTION

ZnO is a semiconductor that is a member of the II–VI wurtzite family and may be deposited in thin film using a number of methods [1]. Since ZnO is electrically conducting and optically transparent in the visible range, thin nano-films of ZnO have found many uses. The most well-known of these uses is as solar cell windows [2]. ZnO may also be more affordable to produce than other commonly used transparent conducting thin films due to its nontoxicity and comparatively abundant supply. Because of their potential applications in field emitters, photodetectors, biosensors, short wavelength light emitting diodes, field emitters, field emitters, ultraviolet laser emission, and information technology. Considerable research endeavors have been undertaken in recent times to fabricate ZnO thin nano-films that possess a high degree of orientation and transparency [3]. ZnO, a semiconductor material belonging to the II-VI group, possesses a significant band gap of 3.3 electron volts at ambient temperature. Additionally, it exhibits a substantial excitonic binding energy of approximately 60 meV. Various applications extensively use ZnO thin nano-films because of their distinctive optical, electrical, and semiconducting characteristic. Despite the adoption of several approaches for the creation

* *Corresponding Author Email: nur.lamis.nassier@uobabylon.edu.iq*

of ZnO thin nano-films, there is still a need to investigate methods for monitoring the shape, size, crystallinity, and various parameters that affect these materials. Consequently, it is imperative to examine the most favorable conditions for the production of ZnO thin coatings that are both transparent and highly oriented [4]. Researchers' main concern is to improve the quality of material stoichiometry. Different methods, such as magnetron sputtering, MOCVD, spray pyrolysis, and pulsed laser deposition (PLD), are employed to produce ZnO thin nano-films [5]. They have garnered particular attention for their potential as power sources. Because of its comparatively simple method, which eliminates the need for a costly vacuum system, and its wide-ranging advantages of big area deposition and uniform film thickness, the sol-gel technique has gained widespread adoption [6]. The sol-gel process offers additional advantages for thin film deposition, including superior stoichiometry control and straightforward doping in film composition. Previous studies have recorded the physical and structural characteristics of ZnO thin nano-films produced via the sol-gel method utilizing various inorganic and/or organic precursors and deposition criteria [7-10]. The optical, vibrational, structural, and photoluminescent characteristics of ZnO thin nano-films synthesized using Sol-gel employing a zinc acetate precursor on a quartz substrate [11].

MATERIALS AND METHODS

Analytical grade reagents were used for chemical synthesis in the current investigation. First, 2-methoxyethanol ($(CH_3)_2CHOH$) was used as a solvent to dissolve the compound zinc acetate dehydrate ($Zn(CH_3COO)_2{\cdot}2H_2O$), and mono-ethanolamine (MEA: $H_2NCH_2CH_2OH$) was added as a stabilizing agent. The zinc acetate concentration was 0.60 mole per liter, and the stoichiometric ratio between zinc acetate and mono ethanolamine (MEA) was kept at 1.0. After stirring the mixture for an hour at 70 °C the end product was a clear, homogeneous solution that could be coated. The application of the coating was carried out using a solution that had been recently prepared. The films on quartz substrates that had been cleaned using ultrasonic methods were created using a spin-coating equipment. For 40 seconds, the device was rotated at a speed of 3000 revolutions/minute. The nano-films were preheated in a furnace for five minutes at 30 °C. This procedure was used to help the solvent evaporate and get rid of any organic residues that could have been left behind. Ten iterations of the spin coating to the preheating method were performed. After that, the nano-films were allowed to anneal for three hours in the air at 500 °C. The categories of the ZnO thin nano-film were identified using the X-ray diffraction method. This was done using an analytical Diffractometer of type PW3710, using Cu Ka radiation (λ = 0.154 nm). The UV-Visible double beam spectrophotometer model (Jasco-V570) was utilized to measure the optical.

Thickness (d) of the films can be determined by applying the formula [12]:

$$d = \frac{\lambda}{2}\frac{\Delta x}{x} \tag{1}$$

in where λ is the incident photon ray's wavelength, Δx is the shifting between the fringes, and x is the fringe width. The fundamental absorption area's absorption coefficient α is found by applying Lambert's law [13]:

$$\alpha = {2.303A}/{t} \tag{2}$$

where (A) is the optical absorbance, and (t) is the thickness of thin film. The following equation gives the extinction coefficient (ko) [14]:

$$k_o = \frac{\alpha\,\lambda}{4\,\pi} \tag{3}$$

The refractive index (n) is defined as the ratio of the innermost part of a substance's velocity (v) to the vacuum (c) velocity of light. Refractive index (n) was determined by plugging the values of reflectance and extinction coefficient (ko) into the following calculation [15]:

$$R = \frac{(n-1)^2 + k_0^2}{(n-1)^2 + k_0^2} \tag{4}$$

Where R is the reflectance.

Also, the refractive index can be expressed through the following equation [15]:

$$n = \left[\left(\frac{1+R}{1-R}\right)^2 - (k_o^2 + 1)\right]^{\frac{1}{2}} + \frac{1+R}{1-R} \tag{5}$$

RESULTS AND DISCUSSION

FESEM results

For the morphological study of material, FESEM

analysis is carried out [16, 17]. The presented FESEM image shows the surface morphology of a zinc oxide (ZnO) thin nano film synthesized via the sol-gel method. The micrograph reveals a highly porous, sponge-like structure characterized by interconnected nanograins and branches (Fig. 1). Such morphology is a typical result of controlled thermal annealing at 500°C, which facilitates the growth of a continuous nanostructured network. This porous texture is indicative of a successful sol-gel process that promotes homogeneous nucleation and results in increased surface area. The nano branches observed are ideal for enhancing surface-dependent properties such as optical absorption and charge transport. This agrees with the optical characterization results reported in the study, where the ZnO films exhibited high UV absorbance (~90%) and a direct optical band gap of 2.84 eV. Furthermore, the grain sizes inferred from the XRD analysis (~20–27 nm) are consistent with the nanoscale features visible in the image. The uniform distribution and compact arrangement of the nanostructures suggest good film crystallinity, which is also confirmed by the XRD peaks aligned with the hexagonal wurtzite phase and preferred orientation along the (002) plane. In conclusion, the FESEM image supports the structural and optical findings of the research, confirming the effective formation of nanostructured ZnO films suitable for applications in solar cells, sensors, and optoelectronic devices [18-22].

XRD results

The crystallinity of material can be determined by XRD study [23-25]. The XRD pattern of ZnO thin film prepared by the sol-gel method on quartz substrates is shown in Fig. 2. All of the diffraction pattern canbe indexed to the hexagonal ZnO phase (Wurtzite Structure) by comparison with thedata from (JCPDS S6-314). However, the XRD patterns of the nanoparticles are considerably broadened due to the very small size of these particles. The strong and narrow diffraction peaks indicated that the product has good crystallinity. The e XRD pattern of ZnO thin nano-films shows three peaks located at 2θ equal 31.800, 34.590

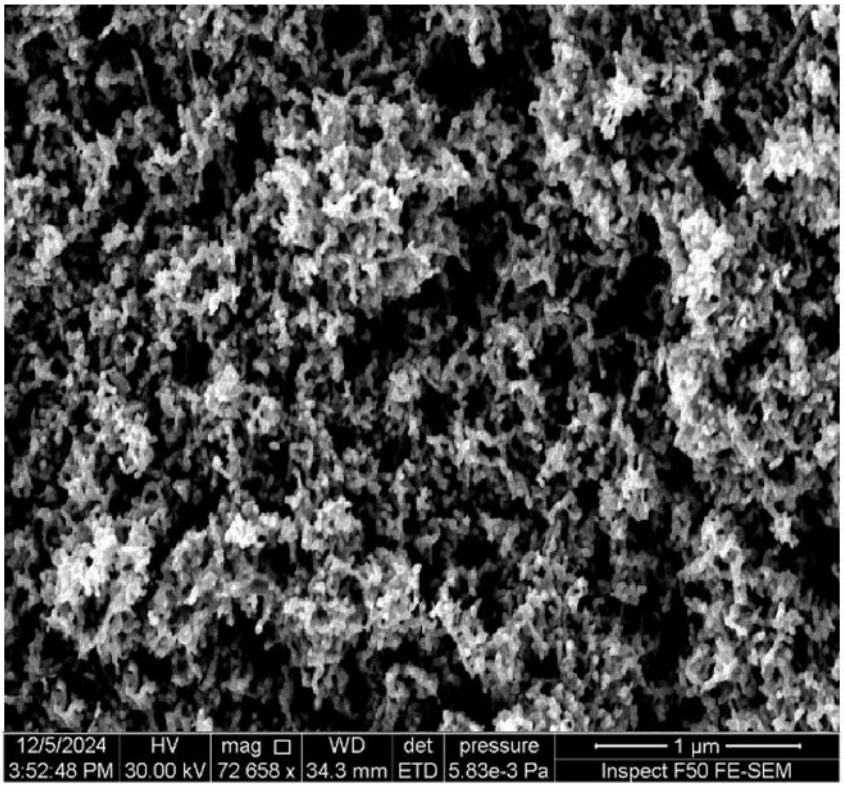

Fig. 1. FESEM Micrograph of Porous ZnO Thin Nano Film Synthesized via Sol-Gel Method at 500°C.

and 36.22 0 corresponding to (100), (101) and (002) planes with prefferd orientation accured at (002) indicating that the films are oriented along c-axis [6, 26, 27]. The typical hexagonal wurtzite structure of thin nano-films is inferred from the XRD pattern. The crystallites sizes (D) of the films

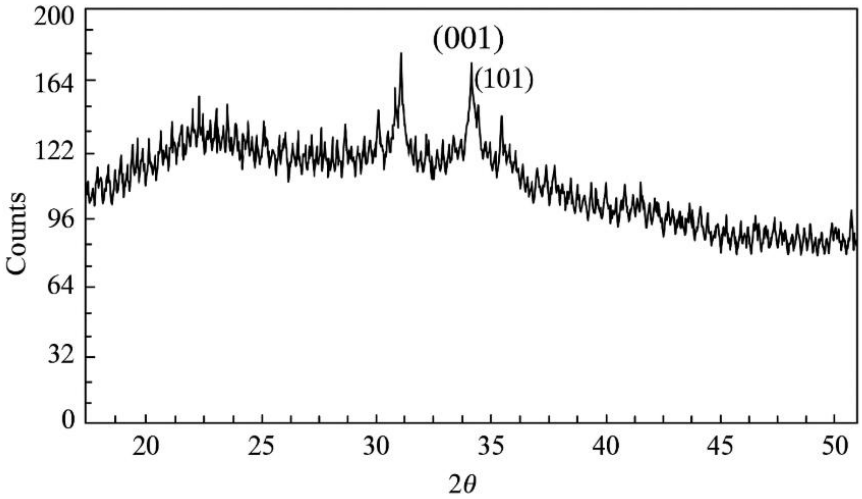

Fig. 2. X-ray Diffraction (XRD) Pattern of ZnO Thin Films Indicating Crystalline Planes and Structural Characteristics.

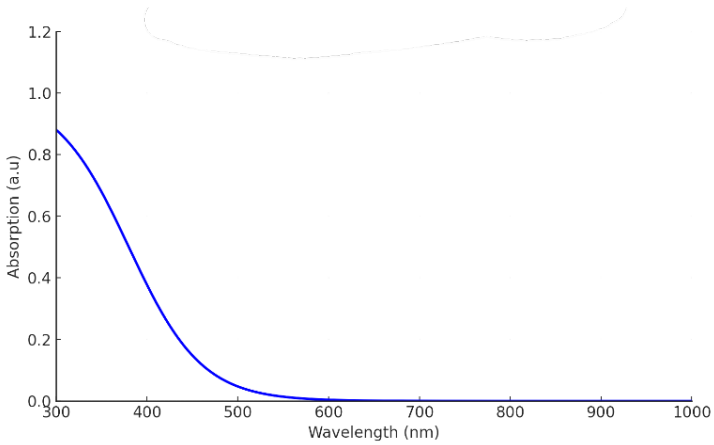

Fig. 3. UV-Visible Absorption Spectrum of ZnO Thin Film.

Table 1. Crystallographic Parameters of ZnO Thin Films: Interplanar Spacing, Crystallite Size, Dislocation Density and Microstrain.

Planes	Interplanar spacing (Å)	FWHM (β) (× 10^{-3} rad.)	Grain size D (nm)	δ (× 10^{14} lines/m²)	ε (× 10^{-3})
(100)	3.805	9.49	20	33.68	3.11
(002)	3.501	7.58	27	19.64	2.83
(101)	3.474	9.49	20	33.68	2.99

are estimated using the Scherer formula [28]:

$$D = \frac{K\lambda}{\beta \cos\theta} \quad (6)$$

where k is the shape factor, which is 0.94. With a Bragg angle 2θ of approximately 34.44˚, λ is the wavelength of the X-ray utilized, which is 1.54 Å, and β is the full width at half maximum of the (002) peak of the XRD pattern.

Fig. 2 shows that peak position is affected by uniform strain, whereas peak broadening and intensity are affected by nonuniform strain. To compute the average strain (***ε***) of nanoparticles, the Stokes-Wilson equation is utilized [28]:

$$\boldsymbol{\varepsilon} = \beta / 4\tan\theta \quad (7)$$

The average grain size is established at 20 nm. The dislocation density (δ), indicative of the quantity of dislocation lines per unit volume, is calculated using the subsequent equation:

$$\delta = \frac{1}{D^2} \quad (8)$$

Table 1 displays the structural characteristics of thin nano-films that have been researched. Based

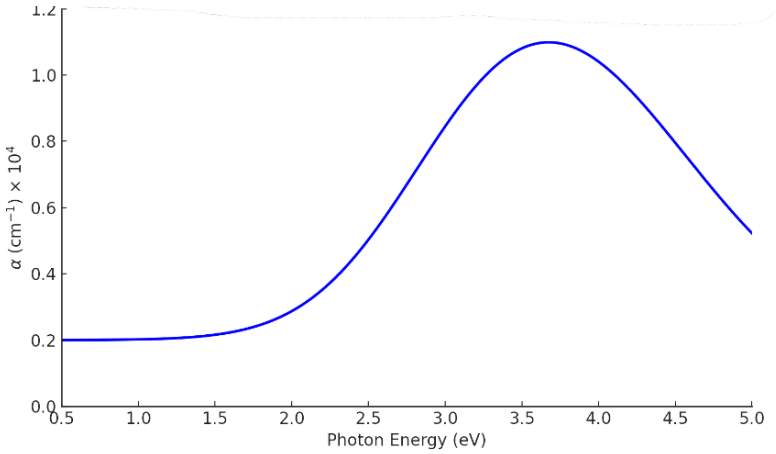

Fig. 4. Absorption coefficient as a function of photon energy of ZnO thin film.

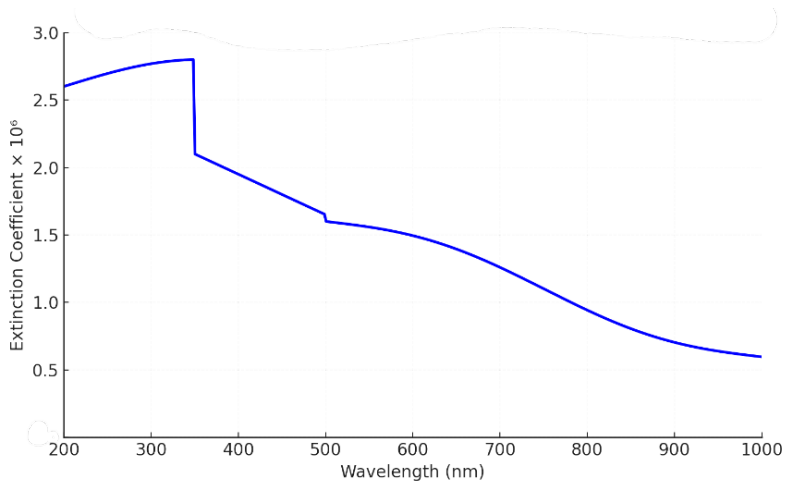

Fig. 5. Extinction coefficient as a function of wavelength of ZnO thin film.

on XRD measurements, the lattice features of ZnO thin nano-films such as dislocation and strain show good agreement with the values provided in (JCPDS S6-314) which agreement with references [29, 30].

Optical properties

The absorption spectra of the ZnO film are depicted in Fig. 3. It is cleared that a high level of absorption in the UV area, followed by a quick drop in the visible region [31].

$$\sigma = \frac{\alpha n c}{4\pi} \quad (9)$$

Where c represents the speed of light. The means of the transformation (indirect or direct) is identified by the relationship [32]:

$$\alpha h\nu = (h\nu - E_g) \quad (10)$$

The energy of a photon is denoted as hv, the band gap energy is represented as Eg, and (r and a)

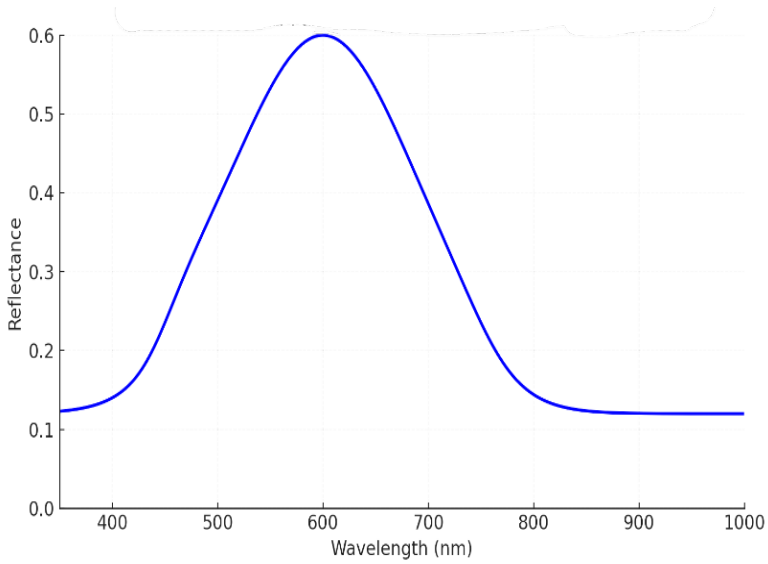

Fig. 6. Reflectance as a function of wavelength of ZnO thin film.

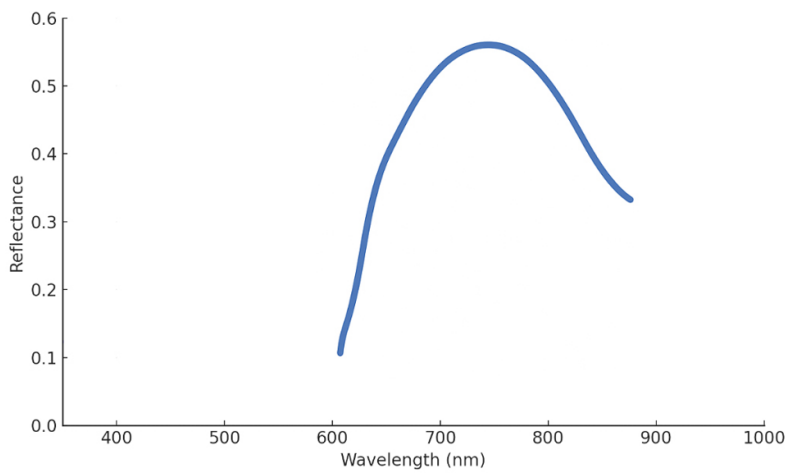

Fig. 7. Variation of (α h ν) ² with photon energy for ZnO thin film.

are constants. It's important to mention because of a permissible direct transition, the value of r is 1/2, while for a permissible indirect transition, the value of r is 3/2. In the near infrared region, the absorption experiments displayed that the created films have very low absorption in the visible range, making them highly suited for the production of solar cells [33, 34].

Fig. 4 displays the absorption coefficient of the ZnO film, as calculated using Eq. 2. The absorption coefficient of this film exhibits a quick increase beyond the absorption edge region, followed by a slow drop due to its inverse relationship with transmittance. It is clear that the ZnO thin film has a greater absorption constant ($\alpha \geq 10^4 cm^{-1}$), which promotes the occurrence of direct transitions [35, 36].

The extinction coefficient (k) has been determined using Eq. 3, and the resulting value is depicted in Fig. 5 for the ZnO film. The extinction coefficient exhibits a quick increase in the UV range, followed by a subsequent decline. Extinction coefficient variation is directly related to light absorption and is expressed as a non-zero value (k) for photon energies below the critical absorption edge.

The ZnO thin film's reflectance spectrum is shown in Fig. 6. As the wavelength grows, the reflectance of the film is seen to rise, peaking at energies that correspond to the film's energy gap. Nevertheless, the reflectance drops with increasing photon energy. The poor absorbance of the film at photon energies and wavelength below the forbidden energy gap is the cause of this phenomenon. An apparent absorbance value is seen when the photon energy is higher than or equal to the energy band gap. This is because the interaction between the material's electrons and the incident photon has sufficient energy to facilitate electronic transitions, and this result is in agreement with [29, 37].

Eq. 7 depicts the refractive index of a ZnO thin film. The connection between the ZnO film's wavelength and refractive index is shown in Fig. 6. When the wavelength rises in the ultraviolet (UV) and the beginning of the visible range, the refractive index values also increase. The data obtained indicate that the produced film has a maximum refractive index value of 1.701%.

Fig. 7 shows that the plot curve is linear, which means that there are direct transitions. It is possible to deduce the direct permissible energy gap of 2.84 eV from the linear connection seen at high photon energy. The results presented here are in agreement with those in References [9, 32].

CONCLUSION

On quartz surfaces, zinc oxide thin nano-films were created using the sol-gel method and 1.0 M zinc acetate solutions. Films have been categorized using structural and optical information. According to the X-ray diffraction analysis, every sample has a hexagonal structure. The sizes of the crystallites are found to be between 20 and 27 nanometers, according to the XRD measurements. The film shows a significant emission peak in the visible range centered at 550 nm, as well as a noticeable emission band at 383 nm. The film exhibits a notable absorption in the ultraviolet spectrum, which rapidly diminishes in the visible and near-infrared areas. The film shows a linear transition with a 2.84 eV permitted energy gap.

ONFLICT OF INTEREST

The authors declare that there is no conflict of interests regarding the publication of this manuscript.

REFERENCES

1. Aleksandrova, M., et al., Ga-Doped ZnO Coating—A Suitable Tool for Tuning the Electrode Properties in the Solar Cells with CdS/ZnS Core-Shell Quantum Dots. Crystals, 2021. 11(2): p. 137.
2. Meftahi, N., et al., Machine learning property prediction for organic photovoltaic devices. npj Computational Materials, 2020. 6(1).
3. Miyake, Y. and A. Saeki, Machine Learning-Assisted Development of Organic Solar Cell Materials: Issues, Analyses, and Outlooks. The Journal of Physical Chemistry Letters, 2021. 12(51): p. 12391-12401.
4. Papadimitropoulos, G., et al., Optical and structural properties of copper oxide thin films grown by oxidation of metal layers. Thin Solid Films, 2006. 515(4): p. 2428-2432.
5. Rajasekaran, M., A. Arunachalam, and P. Kumaresan, Structural, morphological and optical characterization of Ti-doped ZnO nanorod thin film synthesized by spray pyrolysis technique. Materials Research Express, 2020. 7(3): p. 036412.
6. Nassier, L.F. and M.H. Shinen, Study of the optical properties of poly (methyl methacrylate) (PMMA) by using spin coating method. Materials Today: Proceedings, 2022. 60: p. 1660-1664.
7. Onah, D.U., P.A. Nwofe, and H.E. Uguru, Influence of Post-deposition Heat Treatments on the Optical Properties of Chemically Deposited Nanocrystalline TiO2 Thin Films. Research Journal of Applied Sciences, Engineering and Technology, 2016. 13(3): p. 253-256.
8. Ng, S.S., et al., Structural and morphological properties of zinc oxide thin films grown on silicon substrates, in AIP

Conference Proceedings. 2013, AIP. p. 306-309.
9. Abed, z., R. Mohammad, and A. Elttayef, Structural properties of Ag-CuO thin films on silicon prepared via DC magnetron sputtering. Egyptian Journal of Chemistry, 2021. 0(0): p. 0-0.
10. Hamzah, S.K., et al., The Role Caspase-8 and DNA Methylation in patients with Ovarian Cancer: Relationship with Oxidative Stress and Inflammation. Research Journal of Pharmacy and Technology, 2021: p. 2676-2680.
11. Borysiewicz, M.A., ZnO as a Functional Material, a Review. Crystals, 2019. 9(10): p. 505.
12. Galdámez-Martinez, A., et al., Photoluminescence of ZnO Nanowires: A Review. Nanomaterials (Basel, Switzerland), 2020. 10(5): p. 857.
13. Ray, S.C., Preparation of copper oxide thin film by the sol–gel-like dip technique and study of their structural and optical properties. Solar Energy Materials and Solar Cells, 2001. 68(3-4): p. 307-312.
14. Patil, V., et al., Nanocrystalline CuO Thin Films for H₂S Monitoring: Microstructural and Optoelectronic Characterization. Journal of Sensor Technology, 2011. 01(02): p. 36-46.
15. Tombak, A., et al., The novel transparent sputtered p-type CuO thin films and Ag/p-CuO/n-Si Schottky diode applications. Results in Physics, 2015. 5: p. 314-321.
16. Batool, M., M.N. Haider, and T. Javed, Applications of Spectroscopic Techniques for Characterization of Polymer Nanocomposite: A Review. Journal of Inorganic and Organometallic Polymers and Materials, 2022. 32(12): p. 4478-4503.
17. Batool, M., et al., Exploring the usability of Cedrus deodara sawdust for decontamination of wastewater containing crystal violet dye. Desalination and Water Treatment, 2021. 224: p. 433-448.
18. Javed, T., et al., Investigating the adsorption potential of coconut coir as an economical adsorbent for decontamination of lanthanum ion from aqueous solution. Journal of Dispersion Science and Technology, 2024: p. 1-12.
19. Hiroki, A. and M. Taguchi, Development of Environmentally Friendly Cellulose Derivative-Based Hydrogels for Contact Lenses Using a Radiation Crosslinking Technique. Applied Sciences, 2021. 11(19): p. 9168.
20. Savaloni, H. and R. Savari, Nano-structural variations of ZnO:N thin films as a function of deposition angle and annealing conditions: XRD, AFM, FESEM and EDS analyses. Materials Chemistry and Physics, 2018. 214: p. 402-420.
21. Atyaa, A.I., N.D. Radhy, and L.S. Jasim, Synthesis and Characterization of Graphene Oxide/Hydrogel Composites and Their Applications to Adsorptive Removal Congo Red from Aqueous Solution. Journal of Physics: Conference Series, 2019. 1234(1): p. 012095.
22. Kanwal, F., et al., Enhanced dye photodegradation through ZnO and ZnO-based photocatalysts doped with selective transition metals: a review. Environmental Technology Reviews, 2024. 13(1): p. 754-793.
23. Jamel, H.O., et al., Adsorption of Rhodamine B dye from solution using 3-((1-(4-((1H-benzo[d]imidazol-2-yl)amino) phenyl)ethylidene)amino)phenol (BIAPEHB)/ P(AA-co-AM) composite. Desalination and Water Treatment, 2025. 321: p. 101019.
24. Majeed, H.J., et al., Synthesis and application of novel sodium carboxy methyl cellulose-g-poly acrylic acid carbon dots hydrogel nanocomposite (NaCMC-g-PAAc/ CDs) for adsorptive removal of malachite green dye. Desalination and Water Treatment, 2024. 320: p. 100822.
25. Shah, A., et al., Adsorptive removal of arsenic from drinking water using KOH-modified sewage sludge-derived biochar. Cleaner Water, 2024. 2: p. 100022.
26. Sajeesh, S. and C.P. Sharma, Mucoadhesive hydrogel microparticles based on poly (methacrylic acid-vinyl pyrrolidone)-chitosan for oral drug delivery. Drug Delivery, 2010. 18(4): p. 227-235.
27. Shakerimoghaddam, A., et al., Green synthesis and characterization of NiO/Hydroxyapatite nanocomposites in the presence of peppermint extract and investigation of their antibacterial activities against Pseudomonas aeruginosa and Staphylococcus aureus. Results in Chemistry, 2025. 13: p. 101947.
28. Mursal, et al., Structural and Optical Properties of Zinc Oxide (ZnO) based Thin Films Deposited by Sol-Gel Spin Coating Method. Journal of Physics: Conference Series, 2018. 1116: p. 032020.
29. Mohammed, G.H. and H.J. Abdul Karim, Effect of some transitional metal oxides on the structural and optical properties of (ZnO-TiO_2) thin films, in AIP Conference Proceedings. 2021, AIP Publishing. p. 040009.
30. Jassim, D.N., J. Alzanganawee, and G.H. Mohammed, Synthesis and characterization of $(ZnO)_{1-x}$ $(CuO)_x$ films prepared by PLD technique for enhanced the solar cell efficiency. Journal of Optics, 2024.
31. S. Khashan, K., J. A. Saimon, and A. I. Hassan, Optical Properties of Cuo Thin Films with Different Concentration by Spray Pyrolysis Method. Engineering and Technology Journal, 2014. 32(1B): p. 86-93.
32. Khudair, D.Y., et al., Impact of ZnO Atomic Ratio on Structural, Morphological and Some Optical Properties of $(SnO_2)_{1-x}$ (ZnO)x Thin Films. Iraqi Journal of Science, 2020: p. 333-340.
33. Alami, A.H., A. Allagui, and H. Alawadhi, Microstructural and optical studies of CuO thin films prepared by chemical ageing of copper substrate in alkaline ammonia solution. Journal of Alloys and Compounds, 2014. 617: p. 542-546.
34. Jindal, K., M. Tomar, and V. Gupta, CuO thin film based uric acid biosensor with enhanced response characteristics. Biosensors and Bioelectronics, 2012. 38(1): p. 11-18.
35. Omran Alkhayatt, A.H. and S.K. Hussian, Fluorine highly doped nanocrystalline SnO_2 thin films prepared by SPD technique. Materials Letters, 2015. 155: p. 109-113.
36. Maktoof, A.S., G.H. Mohammed, and H.H. Abbas, Effect of annealing process on structural and optical properties of Au-doped thin films (NiO:WO3) fabricated by PLD technique. Journal of Optics, 2024.
37. Davari, F. and M.R. Fadavieslam, The effect of copper doping on the structural, optical, and electrical properties of cadmium oxide thin films using the spray pyrolysis technique. 2021, Research Square Platform LLC.